Polymer Chemistry

Accepted Manuscript

ROYAL SOCIETY OF CHEMISTRY

www.rsc.org/polymers

Journal Name

ARTICLE

Effect of With/Without Resonance-mediated Interactions on the Molecular Weight and Photovoltaic Performance of Polymers with Bis-Tolane as an Integrated Part of the Benzodithiophene Donor Unit for Efficient and Stable Organic Solar Cells

Received 00th January 20xx,
Accepted 00th January 20xx

DOI: 10.1039/x0xx00000x

www.rsc.org/

Nallan Chakravarthi,[†] Kumarasamy Gunasekar,[†] Kakaraparthi Kranthiraja,[†] Taeik Kim,[†] Woosum Cho,[†] Chang Su Kim,[‡] Dong-Ho Kim,[‡] Myungkwan Song,[*,‡] and Sung-Ho Jin[*,†]

With the goal of discovering a new and plausible approach to utilizing the conjugated side chains (CSCs), other than for the previously reported purpose of two-dimensional (2D) π-conjugation extension in π-conjugated polymers, we report, for the first time, the impact of with/without interactions induced via resonance in CSCs on the molecular weight (M_w) and photovoltaic performance of polymers. For this, we designed two donor (D)–acceptor (A) polymers, represented as PBDTBPA(H)-DPP and PBDTBPA(F)-DPP, containing alkoxy-BPA(H) and alkoxy-BPA(F) [BPA = biphenylethynyl] on the benzodithiophene (BDT) unit as novel CSCs, respectively. The introduction of these CSCs generated bis-tolane as an integrated part of the BDT unit, which allowed us to address the difference of the polymerization, photophysical, and photovoltaic properties of PBDTBPA(H)-DPP and PBDTBPA(F)-DPP, as a function of the structural variation of CSC, which has never been investigated in organic solar cells (OSCs). In contrast to the weak electron-donating nature of BPA(H), BPA(F) exhibited a strong electron-donating ability due to the interaction of the lone pair electrons of the fluorine atom with the triple bond via resonance, which decreased the rigidity of the triple bond, whereas in PBDTBPA(H)-DPP the rigidity of the triple bond was retained with no such interaction. The striking differences in the rigidity and different electron-withdrawing tendencies of the CSCs were well correlated with M_w and with the highest occupied molecular orbital (HOMO) energy levels of the polymers. As a result, the inverted OSCs based on PBDTBPA(H)-DPP achieved an open-circuit voltage (V_{oc}) of 0.74 V, and power conversion efficiency (PCE) of 5.58%, which was 38% higher than that of PBDTBPA(F)-DPP-based inverted OSCs. More significantly, the inverted OSC devices were highly stable, retaining 80% of their original PCE after 60-day storage in air, even without encapsulation. To the best of our knowledge, this 5.58% is the highest PCE reported to date for the arylethynyl-substituted BDT donor-based OSCs. These results reveal that bis-tolane [BDTBPA(H)] as an integrated part of the new BDT unit is a promising donor building block for high M_w donor polymers in addition to 2D extended π-conjugation for high performance bulk heterojunction (BHJ) OSCs.

Introduction

Gaining a complete understanding of the relationship between the chemical structure and photovoltaic property of π-conjugated polymer is essential for realizing a higher power conversion efficiency (PCE) for organic solar cells (OSCs) based on bulk heterojunction (BHJ) architecture compared to inorganic solar cells. Until now, much research has been devoted to studying the effect of π-conjugated backbone modification on the band gap, molecular ordering, planarity, thermal stability, and photovoltaic performance of the polymers in both OSC and organic field-effect transistor applications through plausible synthetic strategies.[1-5.]

On the other hand, very few studies have examined the important role played by the conjugated side chain (CSC) in terms of extending the conjugation two dimensionally (2D) and thereby improving the absorption and the charge carrier and photovoltaic parameters. The numerous literature reports on 2D π-conjugated polymers based on benzodithiophene (BDT) have revealed that the CSC located at the upward and downward directions of the BDT unit plays a key role in deciding PCE.[6,7] Moreover, until now only four major CSC functionalities, namely thiophene,[8] selenophene,[9] furan,[10] and phenyl[11] groups, have governed the overall performance of the OSCs based on 2D π-conjugated polymers containing the BDT unit. Regardless of the extraordinary PCE attained, the synthetic complexity involved in further tailoring of these CSCs (aryl/heterocyclic groups) has only confined them as acting as a platform to hold the aliphatic alkyl chains for maintaining solution processibility. In addition, despite the fascinating features of the BDT-based 2D π-conjugated polymers, to the best of our knowledge no successful illustrative report has been published that shows how the subtle variation in the structure of CSC significantly affects the molecular weight (M_w) and the frontier energy levels of the polymer, which in turn affect the charge carrier and photovoltaic properties. This is because the M_w of the polymer plays an important role in improving the charge carrier mobilities and PCE.[12,13] Therefore, the aforementioned issues necessitate further extension of

CSCs with versatile utility for enhancing M_w, modulating frontier energy levels and improving the photovoltaic performance of the polymers rather than just acting for the purpose of 2D conjugation extension.

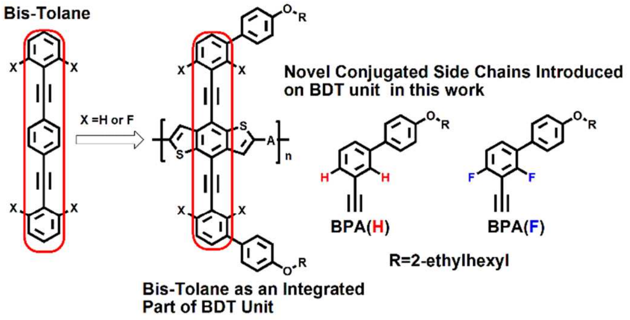

Figure 1. Schematic image of the design strategy of the novel π-conjugated polymers examined in this work.

In the process of our quest for CSCs with multi-functionalities, we specially designed an alkoxy-biphenylethynyl [BPA(H)] group and its fluorinated analogue alkoxy-difluorobiphenylethynyl [BPA(F)] as novel CSCs on the BDT unit, which is entirely different from the routinely introduced heterocyclic/aryl groups. By this simple chemical modification, the structure of our new 2D conjugated BDT-based monomer units BDTBPA(H) and BDTPBA(F) supports to the generation of a new liquid crystal molecule called bis-tolane as an integrated part of BDT in their structures (Figure 1). Structurally, bis-tolane consists of a phenylethynyl group connected to both sides of a benzene ring and it is classes as one of the high birefringence nematic liquid crystals. Bis-tolane-based liquid crystal compounds have been well researched and are recognized as important components for display applications.[14-16] Furthermore, the mesogenic, physical, and chemical properties of these birefringence bis-tolane liquid crystals can be modulated by substitution of hydrogen with fluorine atoms on to the terminal phenyl rings. The dramatic difference in the properties of the liquid crystal compounds with or without fluorine substitution is attributed to the interaction between the lone pair electrons of the fluorine atom and the π-electrons of the triple bond via the resonance effect. Therefore, we envisage that the introduction of such groups as part of the BDT unit will also significantly affect the degree of polymerization, optical properties, and energy levels of the polymers and also the photovoltaic properties of OSCs containing BDT-based 2D π-conjugated polymers.

Based on the aforementioned considerations, this study addresses the impact of with/without interactions induced via resonance effect on the M_w and photovoltaic properties that have been never been reported in OSCs. We designed two donor (D)–acceptor (A) polymers named poly[4,8-bis(4'-(2-ethylhexyloxy)-3-ethynylbiphenyl)benzo[1,2-b:4,5-b']dithiophene]-alt-[2,5-diethylhexl-3,6-bis(5-thiophen-2-yl)pyrrolo[3,4-c]-pyrrole-1,4-dione] (PBDTBPA(H)-DPP) and poly[4,8-bis(4'-(2-ethylhexyloxy)-3-ethynyl-2,4-difluorobiphenyl)benzo[1,2-b:4,5-b']dithiophene]-alt-[2,5-diethylhexl-3,6-bis(5-thiophen-2-yl)pyrrolo[3,4-c]-pyrrole-1,4-dione] (PBDTBPA(F)-DPP) containing BPA(H) and BPA(F) as novel CSCs, respectively (Scheme 1). The fluorine atoms adjacent to the triple bond in PBDTBPA(F)-DPP increased the electron-donating tendency of BPA(F) and reduced the rigidity of the triple bond by an interaction between the lone pair electrons of the fluorine atom with the π-electrons of the triple bond induced via the resonance effect. As a result, PBDTBPA(F)-DPP exhibited a lower degree of polymerization, inferior charge carrier and photovoltaic properties when compared to PBDTBPA(H)-DPP, in which the triple bond character is sustained due to the absence of interactions prompted through the resonance effect. Consequently, under optimized device fabrication conditions, the inverted OSC (IOSC) devices utilizing PBDTBPA(H)-DPP:$PC_{71}BM$ blend exhibited a PCE of 5.58%, which is higher than that of the devices based on the PBDTBPA(F)-DPP:$PC_{71}BM$ BHJ composite. To the best of our knowledge, this is the first report to date demonstrating the high PCE of 5.58% for 2D π-conjugated D–A polymers containing BDT with highly rigid arylethynyl substituents (Table 1). Space charge limited current (SCLC) and atomic force microscopy (AFM) measurements revealed clear correlations of the modified polymer structure via CSC with the carrier mobility, film morphology, and resulting photovoltaic properties.

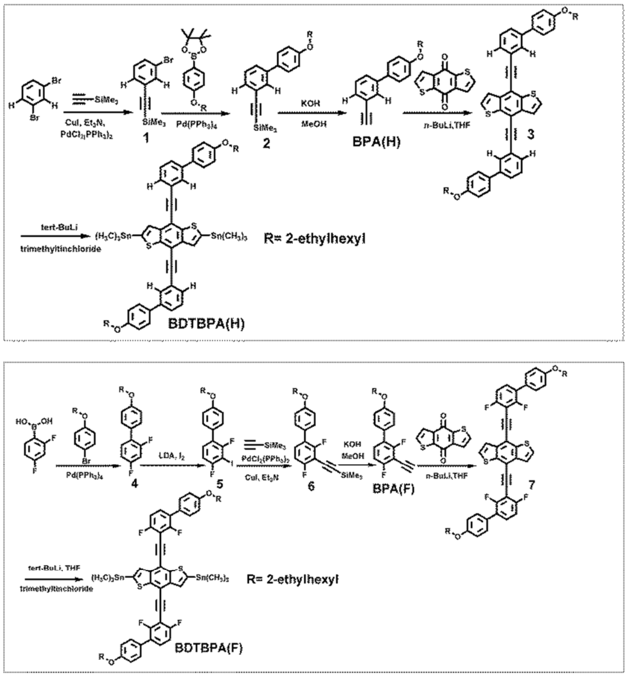

Scheme 1. Synthesis of new CSC groups BPA(H), BPA(F) and the corresponding BDT monomers BDTBPA(H) and BDTBPA(F).

Results and discussion

The electron-rich BDT unit was chosen as a building block to build D–A π-conjugated polymers with the DPP unit (2,5-diethylhexyl-3,6-bis(5-bromothien-2-yl)pyrrolo[3,4-c]-pyrrole-1,4-dione) as a strong electron accepting group because the BDT unit can be functionalized at the 4th and 8th positions, which enables fine tuning of the extended 2D conjugation, solution processability, physical, optical, and electronic properties of the resulting polymers. The two CSCs [BPA(H) and BPA(F)] were attached to the central phenyl ring of the BDT unit with ethylhexyl as a solubilizing group. Bis-tolane, thus generated as an integrated part of the BDT unit by incorporation of those CSCs, allowed us to study the structure-property relationships of the polymers since the triple bond is strongly affected by the substituents with in its vicinity. Compared to the previously reported monomer units with electron-donating (alkyl or alkoxy) substituents,[17] we anticipated that our newly designed BDT monomer units possessing efficient electron delocalization would exhibit overlap of molecular orbitals, irrespective of the substituents adjacent to the triple bond of CSCs. Scheme 1 outlines the synthetic routes of the two new BDT-based donor monomer units, BDTBPA(H) and BDTBPA(F). BPA(H) and BPA(F) were synthesized via various familiar chemical transformations such as Sonogashira and Suzuki coupling, and deprotection under basic conditions. BPA(H) and BPA(F) were reacted with 4,8-dihydrobenzene[1,2-b:4,5-b']dithiophen-4,8-dione to generate the corresponding intermediates 3 and 7, which were subsequently reacted to form BDTBPA(H) and BDTBPA(F), respectively. The Stille coupling polymerizations of the DPP unit and two new donor units, BDTBPA(H) and BDTBPA(F), afforded two D–A polymers PBDTBPA(H)-DPP, PBDTBPA(F)-DPP, respectively, as shown in Scheme 2. The synthetic procedures for the monomers and polymers are explained in detail in the experimental section (Supporting Information). The chemical structures of the monomers were confirmed by ^{1}H and ^{13}C nuclear magnetic resonance (NMR) spectroscopy (Figures S1-S5 in the Supporting Information). The polymers were characterized by ^{1}H NMR (Figure S6 in the Supporting Information) and elemental analysis.

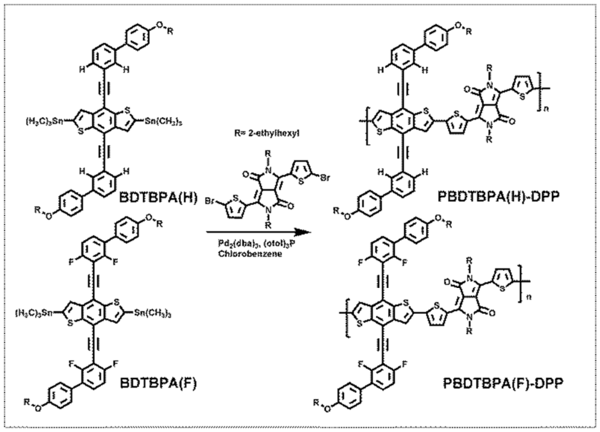

Scheme 2. Synthesis of PBDTBPA(H)-DPP and PBDTBPA(F)-DPP.

Effect of With/Without Resonance-mediated Interactions in CSCs on the Degree of Polymerization and M_w

As encountered in many polymer systems the photovoltaic properties of the polymers were substantially effected by their M_w.[18,19] Hence, we firstly investigated the effect of with/without resonance-induced interactions in CSCs on the M_w of the polymers. Initially, we performed polymerization in a microwave reactor to synthesize PBDTBPA(H)-DPP and PBDTBPA(F)-DPP under the same reaction conditions (chlorobenzene (CB), 120 °C, and 30 min). Surprisingly, PBDTBPA(F)-DPP exhibited less polymerization than PBDTBPA(H)-DPP did, leading to low M_w of 24270 g/mol, even though both polymers contain the rigid triple bond attached to the phenyl group of BDT in both upward and downward directions. Simultaneously, the excessively high M_w of PBDTBPA(H)-DPP afforded an insoluble material that was precipitated out before completion of polymerization under microwave conditions. The difference in M_w and solubility is explained as follows. The triple bond nature in the monomer BDTBPA(H) is not disturbed by the hydrogen's vicinity, making the triple bond more rigid (Figure 2a). In the monomer BDTBPA(F), however, the triple bond nature is perturbed by the interaction by the lone pair electrons of the fluorine atom, and the resulting partial double bond decreases the rigidity (Figure 2b). We tried different reaction conditions such as increasing temperature and time, but failed to increase M_w for PBDTBPA(F)-DPP. To achieve good solubility for PBDTBPA(H)-DPP, we implemented conventional heating polymerization conditions (120 °C, 6 h) and successfully achieved higher M_w for PBDTBPA(H)-DPP than for PBDTBPA(F)-DPP with better solubility. The difference in the degree of polymerization was well correlated with the M_w [M_w of PBDTBPA(H)-DPP > M_w of PBDTBPA(F)-DPP], as shown via gel permeation chromatography (GPC) analysis (Figures S7 and S8). The resulting polymers were cautiously purified through Soxhlet-extracted method using methanol, acetone, and hexane, to remove the impurities and oligomer fractions. Finally, the polymers were extracted into chloroform (CF). The M_w obtained via GPC analysis was 71320 g/mol for PBDTBPA(H)-DPP, which is three times higher than that of PBDTBPA(F)-DPP (M_w of 24270 g/mol). Undoubtedly, this significant difference in M_w will affect the photovoltaic performance in BHJ OSCs based on polymer/[6,6]-phenyl-C_{71}-butyric acid methyl ester ($PC_{71}BM$).[20] Thus far, the majority of reports demonstrating the synthesis of polymers with different M_w (ranging from low to high) were conducted only by changing the reaction conditions such as taking an imbalanced ratio of monomers and solvents with various polarities (Toluene→CB).[12] In a completely different methodology, our design strategy utilizes the structural modification of CSC as a key factor to decide the resultant M_w for the corresponding polymers.

The thermal properties of PBDTBPA(H)-DPP and PBDTBPA(F)-DPP were measured by thermogravimetric analysis (TGA) at a heating rate of 10 °C/min (Figure 3a). The onset of decomposition temperature (T_d, corresponding to 5% weight loss) of PBDTBPA(H)-DPP and PBDTBPA(F)-DPP was 412 and 421 °C, respectively, which demonstrates their excellent thermal stability for OSC application.

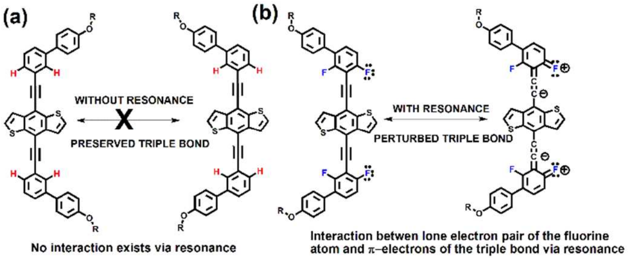

Figure 2. Representative illustration of with/without resonance effect-induced interactions in (a) BDTPBA(H), and (b) BDTPBA(F).

Optical Properties of PBDTBPA(H)-DPP and PBDTBPA(F)-DPP

As mentioned in the above section, the incorporation of BPA(H) or BPA(F) groups on BDT from the upward and downward direction results in the generation of a liquid crystal molecule, i.e., bis-tolane, as an integrated part of the BDT unit. Additionally, the conjugation and polarization of this type of liquid crystal molecule containing bis-tolane derivatives can be significantly enhanced by the lateral substitution with fluorine atoms.[14] Due to the presence of fluorine atoms in the vicinity of the triplebond, the conjugation is not weakened, even when the rings are twisted. This is because the two π-electron pairs of the triple bond are exactly orthogonal to each other. Moreover, a strong interaction exists between the lone pair electrons of the fluorine atom and the π-electrons of the triple bond. Overall, the conjugation and polarization are stronger in fluorinated bis-tolane derivatives than in non-fluorinated bis-tolane derivatives because the lone pair electrons of the fluorine atom restrict the rotation of the phenyl rings via the resonance effect (Figure 2b). In this scenario, we assumed that our newly designed polymers PBDTBPA(H)-DPP and PBDTBPA(F)-DPP, which contain typical molecular features of non-fluorinated and fluorinated bis-tolane, respectively, would also show different optical and electrochemical properties.

Table 1. Comparison of photovoltaic characteristics to previously reported efficiencies of arylethynyl-substituted BDT-based 2D conjugated polymers

Active layer	V_{oc} (V)	J_{sc} (mA/cm^2)	FF (%)	PCE (%)	Ref
PBDTPA-DPP(OD):PC$_{61}$BM	0.45	2.26	39	0.39	29
P1^a:PC$_{61}$BM	0.75	4.00	34	1.05	30
P1^b:PC$_{61}$BM	0.75	5.72	39	1.67	31
PBDTBPA(H)-DPP:PC$_{71}$BM	0.74	13.17	57	5.58	This Work
PBDTBPA(F)-DPP:PC$_{71}$BM	0.68	9.89	50	4.04	This Work

P1^a & P1^b=Poly{4,8-bis(4-decylphenylethynyl)benzo[1,2-b:4,5-b']dithiophene}

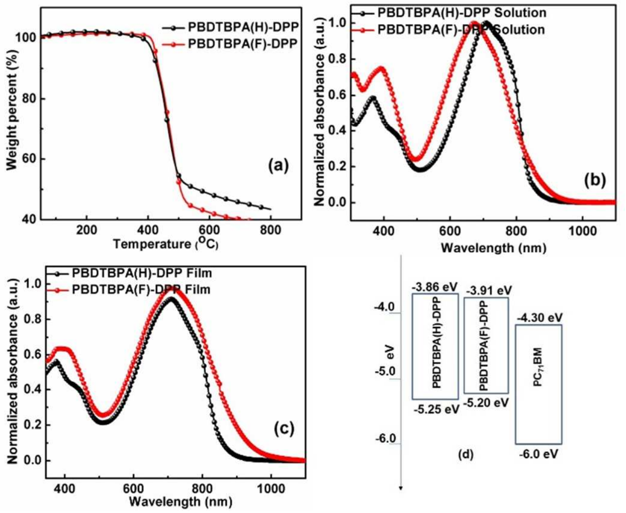

Figure 3. (a) TGA and UV-visible absorption spectra in (b) CF solution, (c) thin film, and (d) HOMO and LUMO energy levels of PBDTBPA(H)-DPP and PBDTBPA(F)-DPP; energy levels of PC$_{71}$BM are shown for comparison.

The optical properties of PBDTBPA(H)-DPP and PBDTBPA(F)-DPP were investigated by measuring the UV–visible absorption spectra of PBDTBPA(H)-DPP and PBDTBPA(F)-DPP in dilute CF solution and in the thin film state, and are shown in Figure 3b and 3c. The absorption maxima (λ_{max}) and optical band gaps (E_g^{opt}) are summarized in Table 2. PBDTBPA(H)-DPP and PBDTBPA(F)-DPP showed two distinct features, a π–π* transition at higher energy region and an intramolecular charge transfer transition at lower energy region, which is a typical feature of D–A π-conjugated polymers. The UV–visible spectrum of PBDTBPA(F)-DPP (λ_{onset} = 961 nm) showed a red shift by 69 nm compared to that of PBDTBPA(H)-DPP (λ_{onset} = 892 nm) in the film states due to the enhanced 2D conjugation induced by the interaction between the lone pair electrons of the fluorine atom and the triple bond in PBDTBPA(F)-DPP. Although this type of interaction was absent in PBDTBPA(H)-DPP due to the absence of lone pair electrons on the hydrogen atom, in turn the CSC core exhibited free rotation which ultimately weakened the conjugation (Figure 2a). The E_g^{opt} of the polymers calculated from the absorption edges was 1.39 eV for PBDTBPA(H)-DPP and 1.29 eV for PBDTBPA(F)-DPP, relatively smaller than the E_g^{opt} values of 1.44 and 1.46 eV for PBDTT-DPP and PBDTP-DPP, respectively,[21] and 1.44 eV for PBDTF-DPP,[10a] indicating that PBDTBPA(H)-DPP and PBDTBPA(F)-DPP have more 2D conjugation in the upward and downward directions than the above mentioned similarly structured polymers but differ in the CSC groups. This is due to the highly conjugated extendable BPA units as CSC groups in the PBDTBPA(H or F)-DPP framework. In the film state, the two polymers display slightly broader spectra that are even further bathochromically shifted compared with those in solution. In contrast to the 3 nm red shift for PBDTBPA(H)-DPP, the thin film spectrum of PBDTBPA(F)-DPP showed a red shift of around 31 nm, indicating that PBDTBPA(F)-DPP possesses a stronger interaction between the polymer chains than does PBDTBPA(H)-DPP in the film state. Even though the E_g^{opt} of PBDTBPA(H)-DPP was 0.1 eV higher than that of PBDTBPA(F)-DPP, the overall spectral coverage of both polymers in the UV–visible spectra demonstrated their potential for use as highly promising candidates for the fabrication of high performance tandem OSCs.

Electrochemical Properties of PBDTBPA(H)-DPP and PBDTBPA(F)-DPP

Cyclic voltammetry (CV) was performed to evaluate the electronic energy levels of the polymers (Figure S9 and Table 2). As shown in Figure 3d, the highest occupied molecular orbital (HOMO) energy levels of PBDTBPA(H)-DPP and PBDTBPA(F)-DPP were estimated to be −5.25 and −5.20 eV, respectively. As shown in Figure 2b, due to the reduction of the triple bond to double bond by the interaction between the lone pair electrons of the fluorine atom and the triple bond via the resonance effect, fluorinated CSC [BPA(F)] behaved as a strong electron-donating group in PBDTBPA(F)-DPP. In contrast, the triple bond nature of non-fluorinated CSC [BPA(H)] remained intact because the absence of

Table 2. Optical and electrochemical properties of PBDTBPA(H)-DPP and PBDTBPA(F)-DPP

Polymer	M_w (g/mol)	$\lambda_{max}{}^a$	$\lambda_{max}{}^b$	$E_g{}^{opt}$ (eV)^c	HOMO (eV)	LUMO (eV)
PBDTBPA(H)-DPP	71320	533	552	1.39	-5.25	-3.86
PBDTBPA(F)-DPP	24270	523	550	1.29	-5.20	-3.91

[a] Absorption maxima measured from UV-visible absorption spectrum in CF solution. [b] Absorption maxima measured from UV-visible absorption spectrum in thin film state. [c] Estimated from the onset of the absorption in thin films ($E_g{}^{opt} = 1240/\lambda_{onset}$).

such interaction made it weaker as an electron-donating group than its fluorinated counterpart. Thus, when BPA(F) was replaced by BPA(H), the HOMO of the polymers was shifted to slightly deeper levels and were anticipated to attain high V_{oc} for the OSCs that contain BPA(H) as CSC. For example, the HOMO of PBDTBPA(H)-DPP was 0.05 eV lower than that of PBDTBPA(F)-DPP. The lower HOMO of the 2D π-conjugated BDT polymers should be favorable for a higher V_{oc} value for the OSCs, since the V_{oc} of the OSCs is interrelated to the difference between the energy levels of the lowest unoccupied molecular orbital (LUMO) of the $PC_{71}BM$ and the HOMO of the polymers.[22] Simultaneously, the LUMO levels for PBDTBPA(H)-DPP and PBDTBPA(F)-DPP were calculated from the HOMO levels attained from the CV analysis and the $E_g{}^{opt}$ ($E_{LUMO} = E_{HOMO} + E_g{}^{opt}$). Accordingly, the LUMO levels were −3.86 and −3.91 eV for PBDTBPA(H)-DPP and PBDTBPA(F)-DPP, respectively.

Investigation of the Photovoltaic Properties of PBDTBPA(H)-DPP and PBDTBPA(F)-DPP

To understand the importance of the impact of with/without resonance-mediated interactions in CSCs on PCE, the corresponding photovoltaic devices were examined by fabricating BHJ OSCs with an inverted device architecture of ITO/ZnO/polymer:$PC_{71}BM$/PEDOT:PSS/Ag by using PBDTBPA(H)-DPP and PBDTBPA(F)-DPP as the electron donor materials and $PC_{71}BM$ as the standard electron acceptor material.[23a] Due to the strong ability to absorb more light in the visible range, $PC_{71}BM$ was selected as the electron acceptor material as an alternative to $PC_{61}BM$. The device optimization process contained careful adjustment of the blend ratios ranging from 1:0.7 to 1:2 in CB and the solvent additives[23b]. Finally, the ratio and solvent system for both polymers were optimized at 1:1.5 and CB+3% 1,8-diiodooctane (DIO), respectively. For further improving PCE, we implemented the methanol treatment method as part of our device process. The current density–voltage (*J*–*V*) curves of pristine polymer:$PC_{71}BM$ devices at different ratios are shown in Figure S10a and S10b and the related data are shown in Table S1. The *J*–*V* curves of pristine polymer:$PC_{71}BM$ devices with 3% DIO and methanol treatment at the blend ratio of 1:1.5 are presented in Figure 4a and 4b and the detailed data are collected in Tables 3 and 4. The devices using PBDTBPA(H)-DPP processed from CB+3%DIO exhibited the highest PCE of 4.62% with a large V_{oc} of 0.73 V, short−circuit current density (J_{sc}) of 12.36 mA/cm^2 and fill factor (FF) of 51.21%. In contrast, under the same processing conditions, the device using PBDTBPA(F)-DPP exhibited a low PCE of 3.04% with a V_{oc} of 0.68 V, J_{sc} of 9.49 mA/cm^2, and FF of 46.99%. From these photovoltaic characteristics, we inferred that the IOSCs based on the PBDTBPA(F)-DPP containing fluorine atoms in the CSC exhibited inferior photovoltaic properties to those of the IOSCs based on the PBDTBPA(H)-DPP containing non-fluorine atoms in the CSC.

We next examined the correlation between structural modification and the photovoltaic properties of the IOSC devices based on PBDTBPA(H)-DPP and PBDTBPA(F)-DPP. The interaction between the lone pair electrons of the fluorine atom and the triple bond in the CSC is solely responsible for the decreased V_{oc}, J_{sc}, and FF of the PBDTBPA(F)-DPP-based IOSCs compared to those of PBDTBPA(H)-DPP. Compared to PBDTBPA(F)-DPP with V_{oc} of 0.68 V, PBDTBPA(H)-DPP showed a substantially improved V_{oc} of 0.74 V, which was attributed to the well-maintained triple bond nature in PBDTBPA(H)-DPP due to the presence of hydrogen atoms with no lone pair electrons to interact with the triple bond via resonance. For PBDTBPA(F)-DPP, the triple bond nature is perturbed by the interaction of the lone pair electrons of the fluorine atom acquiring a partial double bond character (Figure 2b). Consequently, the HOMO level of PBDTBPA(H)-DPP is deepened compared to that of PBDTBPA(F)-DPP due to the restored electron-withdrawing nature of the triple bond in PBDTBPA(H)-DPP.

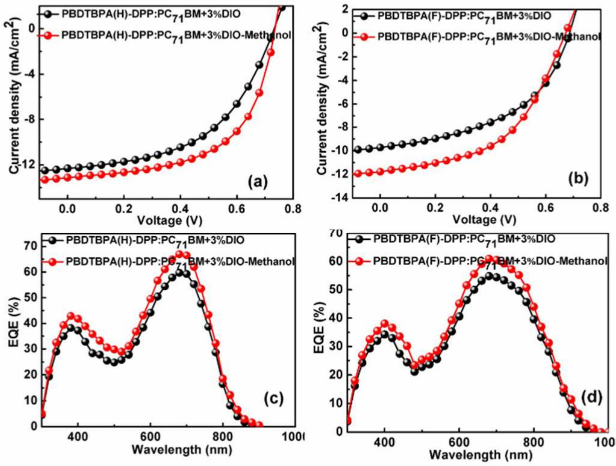

Figure 4. Current density-voltage (*J-V*) and EQE curves of the IOSCs based on PBDTBPA(H)-DPP and PBDTBPA(F)-DPP at the blend ratio of 1:1.5 under optimized and methanol-treated conditions.

The $E_g{}^{opt}$ values of PBDTBPA(H)-DPP and PBDTBPA(F)-DPP suggest that PBDTBPA(F)-DPP-based devices should provide higher photocurrent densities than PBDTBPA(H)-DPP-based devices, since the $E_g{}^{opt}$ of PBDTBPA(F)-DPP was smaller than that of PBDTBPA(H)-DPP. Surprisingly, however, J_{sc} of the PBDTBPA(H)-DPP-based IOSCs was significantly higher than that of PBDTBPA(F)-DPP. The improved J_{sc} for PBDTBPA(H)-DPP (12.36 mA/cm^2) compared to that of PBDTBPA(F)-DPP (9.49 mA/cm^2) was correlated to the M_w of the polymers [M_w of PBDTBPA(H)-DPP> M_w of PBDTBPA(F)-DPP]. The higher M_w of PBDTBPA(H)-DPP compared to that of PBDTBPA(F)-DPP has

Table 3. Photovoltaic properties of polymer:$PC_{71}BM$ BHJ IOSCs at a blend ratio of 1:1.5 processed from CB and (with or without) DIO

polymer	3% DIO	J_{sc} (mA/cm^2)	V_{oc} (V)	FF (%)	R_s (Ω.cm^2)	PCE (%)	Integrated J_{sc} (mA/cm^2)
PBDTBPA(H)-DPP	No	8.22±0.10	0.72±0.01	49.32±1.67	17.63±0.21	2.88±0.05	8.10±0.12
PBDTBPA(H)-DPP	Yes	12.36±0.10	0.73±0.01	51.21±0.70	7.31±0.15	4.62±0.10	12.06±0.10
PBDTBPA(F)-DPP	No	7.71±0.42	0.66±0.03	37.89±1.68	35.23±0.78	1.92±0.10	7.31±0.20
PBDTBPA(F)-DPP	Yes	9.49±0.16	0.68±0.01	46.99±1.03	16.82±1.20	3.04±0.16	9.29±0.13

[a]PCE is average of 10 IOSCs.

already been explained from a structural point of view in the earlier section. In line with the earlier reports, the high M_w of PBDTBPA(H)-DPP accounts for the enhanced J_{sc} of the corresponding PBDTBPA(H)-DPP-based IOSCs. Tables 3 and 4 show that FF also steadily increased in parallel to the trends for V_{oc} and J_{sc} for PBDTBPA(H)-DPP-based devices, possibly due to increased mobility (*vide infra* in next sections), which decreases the charge recombination.[24]

The PCE of PBDTBPA(H)-DPP and PBDTBPA(F)-DPP-based IOSCs was further enhanced by post-deposition polar solvent treatment.[25-28] Encouragingly, after treating the photoactive layer with methanol, the BHJ composites of PBDTBPA(H)-DPP and PBDTBPA(F)-DPP efficiently reciprocated to the methanol treatment, and the PCEs of all IOSCs were dramatically enhanced to 5.58 and 4.04% for the IOSCs based on PBDTFBPA(H)-DPP and PBDTFBPA(F)-DPP, respectively. The highest efficiency of 5.58 %, with a V_{oc} of 0.74 V, J_{sc} of 13.17 mA/cm^2, and FF of 57.28 %, was obtained from the IOSCs based on PBDTBPA(H)-DPP. This efficiency enhancement attained by simple methanol treatment suggests the possibility of further improving PCE with the electrode and active layer interface engineering by several proposed strategies.[13] However, even after methanol treatment, the photovoltaic properties of PBDTBPA(H)-DPP-based devices were superior to those of PBDTBPA(F)-DPP. We attributed the enhanced PCE for PBDTBPA(H)-DPP upon methanol treatment to its high M_w compared to PBDTBPA(F)-DPP. Furthermore, the PCE of 5.58% is highest value ever reported for polymers containing BDT with arylethynyl substituents.[29-31]

The PCE data demonstrated the effectiveness, in comparison with other research reports, of our molecular design strategy of introducing bis-tolane as an integrated part of the BDT unit.[7,8] Those literature reports disclosed that the opto-electronic, photovoltaic, and morphological properties of the polymers entirely depend on the dihedral angles between the BDT unit and CSCs. However, according to hybrid orbital theory, the electron-donating tendency of the triple bond is weak when compared to the frequently used aryl/heterocyclic groups, which is beneficial for maintaining deeper HOMO levels for higher V_{oc}. In addition, the triple bond possesses high rigidity compared to the aryl/heterocyclic substituents, which allows the polymers to obtain a higher Mw that is advantageous for higher charge carrier mobility and proper phase separation in BHJ devices. Although highly respectable PCE was achieved in the case of aryl/heterocyclic substituted BDT donor-based OSCs, the design approach of the polymers was confined to merely changing the aliphatic side chains on them due to the synthetic complexity for further structural modification.[32] In contrast, our molecular design undoubtedly differs from the other reported strategies in terms of the introduction of CSCs [BPA(H) or BPA(F)] on the BDT unit, as the CSC groups serves not only to extend the conjugation in vertical directions, but also to offer further gains in the development of high M_w polymers. With regards to the synthetic flexibility of the triple bond, it is possible to produce a variety of CSCs for introduction on the BDT unit for further expansion of efficient 2D π-conjugated polymers with high M_w. Overall, the elegant molecular design and device fabrication methodologies presented herein enabled us to attain a high PCE of 5.58%, which has never been reported elsewhere for polymers containing highly rigid triple bond as CSC on the BDT unit.

To further increase the relative efficiency of the IOSCs based on PBDTBPA(H)-DPP compared to those based on PBDTBPA(F)-DPP, the external quantum efficiencies (EQE) of the IOSCs were measured and compared. Figures 4c, 4d and S10c, S10d present the EQE curves of the IOSCs based on PBDTBPA(H)-DPP and PBDTBPA(F)-DPP under different processing conditions. The EQE ranged from 350 to 950 nm, which is in good agreement with the absorption spectra of PBDTBPA(H)-DPP and PBDTBPA(F)-DPP (Figure 3c). Interestingly, after treating the photoactive layer with methanol, EQE was considerably increased for the IOSCs based on PBDTBPA(H)-DPP and PBDTBPA(F)-DPP, which was

Table 4. Photovoltaic properties of BHJ IOSCs based on polymer:PC$_{71}$BM at a blend ratio of 1:1.5 processed from CB with methanol treatment

Polymer	J_{sc} (mA/cm^2)	V_{oc} (V)	FF (%)	R$_s$ (Ω.cm^2)	PCE^a (%)	Integrated J_{sc} (mA/cm^2)
PBDTBPA(H)-DPP	13.17±0.12	0.74±0.01	57.28±1.59	4.10±0.36	5.58±0.25	12.86±0.22
PBDTBPA(F)-DPP	11.81±0.10	0.68±0.01	50.53±0.29	9.89±0.65	4.04±0.07	11.47±0.29

^{a}PCE is average of 10 IOSCs.

consistent with the photocurrent values. However, increased EQE from the IOSCs based on PBDTBPA(H)-DPP raised the expectation for high hole mobility and a proper BHJ phase separation for PBDTBPA(H)-DPP, which can assist in increasing J_{sc} and FF. The J_{sc} values calculated from the integration of the EQE spectra were well matched with J_{sc} obtained from the J–V measurements, considering the common error of 5-10% (Tables 3 and 4). Overall, the EQE of the IOSC based on PBDTBPA(H)-DPP (Figure 3b) was in good compliance with the enhanced J_{sc} and FF as the EQE increased compared to the IOSC based on PBDTBPA(F)-DPP. As shown in Figure S11, the dark current J–V curves of the IOSCs based on both PBDTBPA(H)-DPP and PBDTBPA(F)-DPP with methanol treatment exhibited a high R$_{sh}$ and low R$_s$ compared to the case without methanol treatment. For instance, the R$_{sh}$ values were calculated to be 7.65×105 Ω·cm^2 and 3.2 ×105 Ω·cm^2 for with and without methanol-treated IOSCs based on PBDTBPA(H)-DPP, respectively. Moreover, the R$_s$ of the methanol-treated IOSCs was 4.10±0.36 Ω·cm^2, which was lower than that of the pristine IOSCs (7.31±0.15 Ω·cm^2). This result supports the promise of reduced leakage current and better charge collection efficiency due to the high rectification ratio (higher R$_{sh}$ and low R$_s$).[33]

Morphological Studies

To investigate the correlation between the enhanced M$_w$ via structural modification of CSCs and the morphological features in the polymer thin films, we implemented tapping mode AFM to investigate the morphologies of the polymer:PC$_{71}$BM thin films. The thin film morphologies of PBDTBPA(H)-DPP:PC$_{71}$BM and PBDTBPA(F)-DPP:PC$_{71}$BM BHJ composites in optimized and methanol-treated conditions are shown in Figure 5a, 5c and 5b, 5d, respectively. PBDTBPA(H)-DPP exhibited relatively good film forming ability with root-mean-square (RMS) surface roughness of 6.1 nm, compared to 6.9 nm for PBDTBPA(F)-DPP in their pristine blend films (Figure S12). Furthermore, a smooth film morphology was observed from the AFM height images of PBDTBPA(H)-DPP:PC$_{71}$BM in the presence of 3%DIO and methanol treatment. This smooth morphology is beneficial for charge separation and transport within the BHJ composite, which leads to higher J_{sc} due to a larger interface area between PBDTBPA(H)-DPP and PC$_{71}$BM domains. However, the AFM images of the PBDTBPA(F)-DPP:PC$_{71}$BM-based films in 3%-DIO and methanol treatment conditions indicated non-uniform morphological conditions with increased RMS roughness compared to the PBDTBPA(F)-DPP:PC$_{71}$BM-based devices. The large phase separation afforded an aggregated morphology for PBDTBPA(F)-DPP:PC$_{71}$BM composite, which in turn created an unfavorable condition for efficient exciton dissociation, leading to lower J_{sc}. We also observed the M$_w$-dependent morphology adjustment for our BHJ IOSC film composites, which is in agreement with the previous reports.[24] Upon methanol treatment, the PBDTBPA(H)-DPP:PC$_{71}$BM BHJ composite showed improved morphological characteristics (RMS = 1.5 nm) compared to the PBDTBPA(F)-DPP:PC$_{71}$BM BHJ composite (RMS = 3.2 nm), which revealed the smoother morphology obtained in the former BHJ composite.

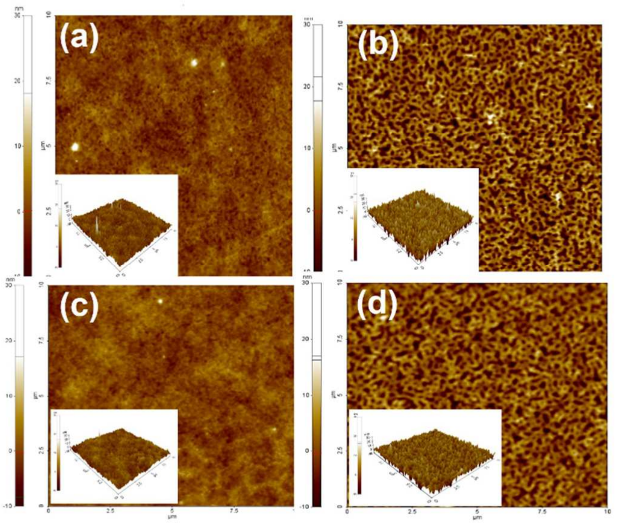

Figure 5. AFM images of (a) PBDTBPA(H)-DPP:PC$_{71}$BM (1:1.5) + 3%DIO, (b) PBDTBPA(F)-DPP:PC$_{71}$BM (1:1.5) + 3%DIO, (c) PBDTBPA(H)-DPP:PC$_{71}$BM (1:1.5) + 3%DIO (methanol), and (d) PBDTBPA(F)-DPP:PC$_{71}$BM (1:1.5) + 3%DIO (methanol).

Correlating the AFM images to the device data implies that the PBDTBPA(F)-DPP with the fluorinated CSC unit produces a large

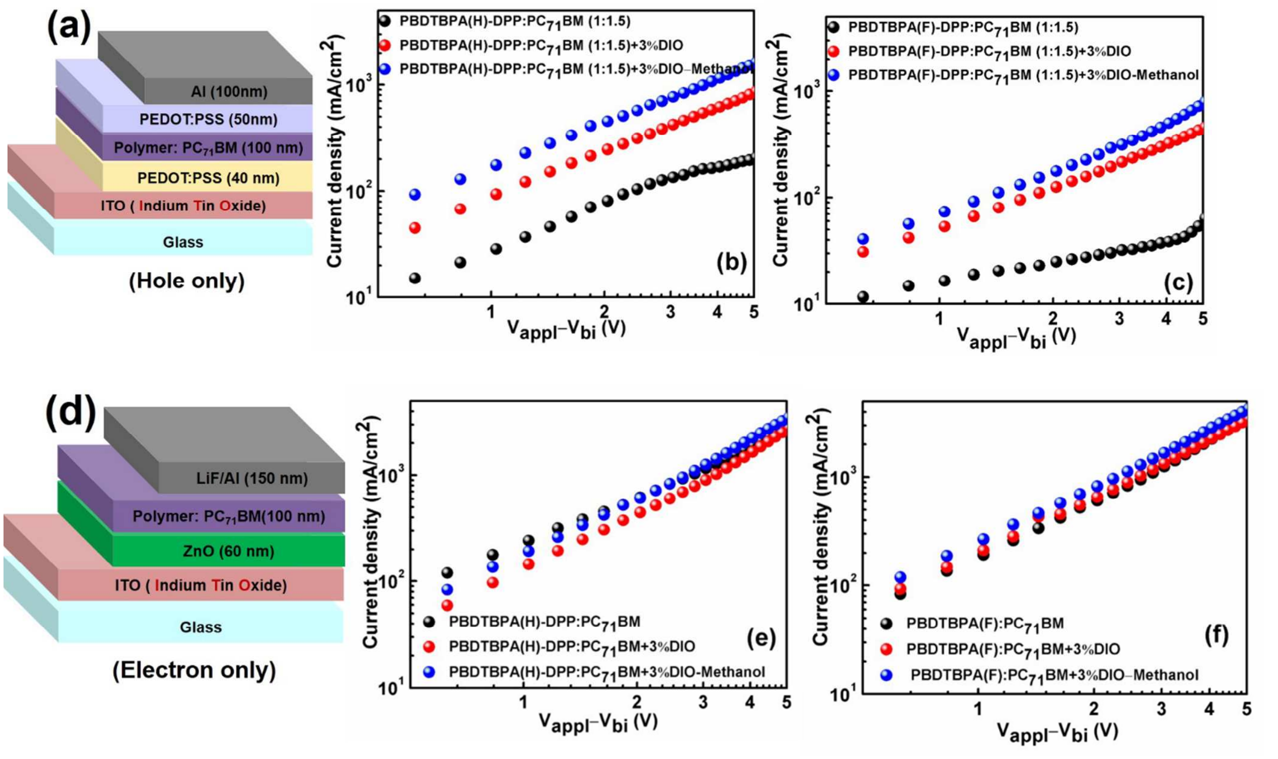

Figure 6. Schematic diagram of hole-only and electron-only device structure and the corresponding current density-voltage (J-V) curves at the blend ratio of 1:1.5.

phase separation from the BHJ composites, inducing less efficient charge carrier transport and thus delivering low J_{sc}, whereas the morphology of PBDTBPA(H)-DPP-based IOSC devices affords a better morphological feature and provides more charge carriers.

X-ray diffraction (XRD) measurement was performed to examine the crystalline properties of thin films of PBDTBPA(H)-DPP and PBDTBPA(F)-DPP. As the XRD patterns of the polymers casted from CF shown in the Figure S13, weak diffraction peaks for π−π stacking of the polymers can be noticed. The PBDTBPA(F)-DPP shows a peak at 2θ = 22.4°, corresponding to a π−π stacking d-spacing of 3.96 Å; but the PBDTBPA(H)-DPP films show diffraction peaks at ca. 20.9°, which is corresponding to d-spacing of 4.25 Å. As per the XRD results, PBDTBPA(F)-DPP shows more strong π−π stacking than PBDTBPA(H)-DPP. The results of XRD is well correlated with the morphological studies (mentioned above), that relatively large aggregates are formed in the PBDTBPA(F)-DPP:PC$_{71}$BM blend compared to the PBDTBPA(H)-DPP:PC$_{71}$BM blend, which can be attributed to the strong interchain π−π stacking effect of the PBDTBPA(F).[6] Therefore, higher charge carrier mobility is anticipated from the IOSCs based on PBDTBPA(H)-DPP compared to those based on PBDTBPA(F)-DPP.

Effect of M$_w$ on the Charge Carrier Mobility

To gain further insight into the influence of M$_w$ on the enhanced J_{sc}, FF and PCE, the charge transport properties were investigated using the SCLC model. Before investigating the effect of M$_w$ on the hole mobility (μ_h) of the BHJ composites, we primarily measured and compared μ_h of the bare polymers (Figure S14) with the configuration of ITO/PEDOT:PSS/polymer/MoO$_3$/Al. The SCLC study revealed that PBDTBPA(H)-DPP displayed an increased μ_h of 3.84x10^{-4} cm^{2}V^{-1}s^{-1} (M$_w$=71320 g/mol), which was 2.5-fold higher than that of PBDTBPA(F)-DPP with μ_h of 1.53x10^{-4} cm^{2}V^{-1}s^{-1} (M$_w$=24270 g/mol). This is in good agreement with the previous reports on the correlation between M$_w$ and μ_h.[12,24,34] The enhanced μ_h for PBDTBPA(H)-DPP probably originated from the higher M$_w$, as determined from the GPC study, due to the preserved rigidity of the triple bond resulting from the absence of the interactions induced via the resonance effect

(Figure 2a). We also measured the hole-only (ITO/PEDOT:PSS/polymer:PC$_{71}$BM/PEDOT:PSS/Ag) and electron-only (ITO/ZnO/polymer:PC$_{71}$BM/LiF/Al) mobility of the BHJ composites using the SCLC model, and the J−V characteristics are plotted in Figure 6. The related data are summarized in Table S2. The calculated μ_h for the PBDTBPA(H)-DPP:PC$_{71}$BM device (6.55x10^{-5} cm^{2}V^{-1}s^{-1}) was double that of the PBDTBPA(F)-DPP:PC$_{71}$BM device (3.37x10^{-5} cm^{2}V^{-1}s^{-1}), which we attributed to the better percolation pathways (ordered network of PBDTBPA(H)-DPP chains) induced via the better morphological conditions obtained in the PBDTBPA(H)-DPP-based BHJ composite, which improved the charge transportation throughout the device. The calculated electron mobilities (μ_e, cm^{2}V^{-1}s^{-1}) were nearly identical (Table S2), despite the large variation between the μ_h of the IOSC devices based on PBDTBPA(H)-DPP and PBDTBPA(F)-DPP. Consequently, the mobility ratio (μ_h/μ_e) was highest in the PBDTBPA(H)-DPP:PC$_{71}$BM BHJ composite. Therefore, the efficient charge transport in the PBDTBPA(H)-DPP-based BHJ composite was attributed to the increased mobility ratio, which reduced the number of space charges in the IOSC device based on PBDTBPA(H)-DPP.[35] The same hole mobility trend was observed even after methanol treatment, which confirmed the superiority of PBDTBPA(H)-DPP over PBDTBPA(F)-DPP as a polymer. Overall, the charge carrier studies revealed that achieving high M$_w$ for the polymers is a prerequisite to acquiring high J_{sc} for corresponding IOSC devices. In this case, our design strategy of introducing BPA(H) as CSC on the BDT unit for maintaining the rigidity of the triple bond was highly advantageous for increasing M$_w$, as was well demonstrated by the SCLC study results.

Impedance Study

To further support the phenomenon of PCE improvement of the IOSCs based on PBDTBPA(H)-DPP and PBDTBPA(F)-DPP after methanol treatment, electrical impedance spectroscopy (EIS) was performed to investigate the detailed electrical properties of IOSCs, which could not be examined by direct current measurements. The internal resistance of the IOSCs measured via EIS is composed of the sheet resistance (R_{SH}) of the electrodes, and the charge-transport resistance (R_{CT}) at the photoactive layer/electrodes interfaces and inside the photoactive layer. In the case of with and without methanol treatment conditions, the R$_{sh}$ of all IOSCs was the same for both the ZnO/ITO cathode and the Ag anode for the IOSC devices based on PBDTBPA(H)-DPP and PBDTBPA(F)-DPP. Thus the variation in internal resistance of the whole device originated from inside the photoactive layers, which were processed from methanol treatment. Figure S15 shows the Nyquist plot of all IOSCs, both with and without methanol treatment. The EIS analysis revealed that the internal resistance of the IOSCs based on PBDTBPA(H)-DPP using methanol treatment was ca. 54 Ω, which was much smaller than the value of ca. 159 Ω for the IOSCs without methanol treatment. These data suggested that the methanol treatment can improve the contact between the photoactive layer and the top Ag electrode and, consequently, facilitate the charge transport in IOSCs, resulting in high J_{sc}, FF, and PCE. This indicates that simple post solvent treatment methods such as methanol treatment could be effective and affordable in fabricating outstanding OSCs when compared to other more burdensome device processing techniques. Further, the Nyquist plots also clearly revealed a significant reduction in resistance of the IOSC devices based on PBDTBPA(H)-DPP compared to PBDTBPA(F)-DPP, which was well correlated with the enhanced J_{sc} and FF for PBDTBPA(H)-DPP.

Investigation of IOSCs Stability

Along with other photovoltaic parameters, stability is a very important factor in the commercial application of OSCs. With this objective, we investigated the stability of the IOSCs in terms of PCE for a period of 60 days. As shown in Figure 7, the IOSCs primarily displayed good performance with a PCE of 5.58 and 4.00% for PBDTBPA(H)-DPP and PBDTBPA(F)-DPP, respectively. After 60-day storage in ambient conditions, the devices still exhibited a high PCE of 4.65 and 3.20%, respectively, which equated to a retention of 80% of their highest efficiency. The better stability of the IOSCs based on PBDTBPA(H)-DPP and PBDTBPA(F)-DPP supports our study recommendation of these polymers with bis-tolane as an integrated part of the BDT unit as a promising material for large scale OSC application. Their stability can be further improved if the devices are well encapsulated.

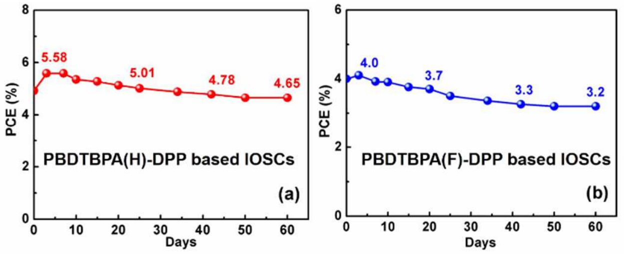

Figure 7. Stability of the IOSCs based on PBDTBPA(H)-DPP and PBDTBPA(F)-DPP.

Conclusions

To examine the impact of with/without resonance-mediated interactions in CSCs, PBDTBPA(H)-DPP and PBDTBPA(F)-DPP, two polymers with bis-tolane as an integrated part of the BDT unit, were designed and synthesized with different CSC groups [BPA(H) and BPA(F), respectively] incorporated on the BDT unit. These two novel CSCs, with [BPA(F)] and without [BPA(H)] fluorine atom adjacent to the triple bond on the BDT unit, offered the opportunity to modify the polymerization, optical, electrochemical, charge carrier, and photovoltaic properties of the polymers. PBDTBPA(F)-DPP with fluorinated CSC [BPA(F)] displayed weaker triple bond rigidity than PBDTBPA(H)-DPP with non-fluorinated CSC [BPA(H)], which significantly affected the degree of polymerization [M$_w$ of PBDTBPA(H)-DPP > M$_w$ of PBDTBPA(F)-DPP]. The decreased rigidity of the triple bond in CSC with fluorine atoms was due to an interaction induced between the lone pair electrons of the fluorine atom and the triple bond via the resonance effect. In contrast to the strong electron-withdrawing tendency of the non-fluorinated CSC of PBDTBPA(H)-DPP, PBDTBPA(F)-DPP substituted with fluorinated CSC possessed a strong electron-donating tendency. As a result, the HOMO of PBDTBPA(H)-DPP was deepened, resulting in a high V_{oc} of 0.74 V for the IOSCs based on PBDTBPA(H)-DPP, compared to 0.68 V for PBDTBPA(F)-DPP. Furthermore the μ_h, PCE and morphology of the IOSCs based on PBDTBPA(H)-DPP and PBDTBPA(F)-DPP strongly correlated with their M_w. The PCE of 5.58% for PBDTBPA(H)-DPP is the highest value reported to date for arylethynyl substituted BDT-based polymers with simple inverted device structure and high device stability. Moreover, the high stability of the IOSCs was proved by their ability to maintain 80% of their maximum PCE after 60 days of air storage under unencapsulated conditions. Therefore, bis-tolane as an integrated part of the BDT unit has great potential for application as a novel electron-rich building block, not only for extending the conjugation in vertical directions but also for realizing high polymers. The PCE of the D−A polymers containing bis-tolane [BDTBPA(H)] as an integrated part of the BDT unit can be further improved by polymerizing with different electron deficient units, which offers scope to increase V_{oc}, J_{sc}, FF further, in addition to the use of various device fabrication methods such as incorporating buffer layers in the device to improve interfacial features that are currently under investigation in our laboratory. Therefore, this study has increased our understanding of the molecular design of high M_w polymers by means of new CSCs along with 2D conjugation extension for efficient large-area OSCs.

Acknowledgements

This work was supported by grant fund from the National Research Foundation (NRF) (2011-0028320) and the Pioneer Research Center Program through the NRF (2013M3C1A3065522) by the Ministry of Science, ICT & Future Planning (MSIP) of Korea.

Notes

[†] *Department of Chemistry Education, Graduate Department of Chemical Materials, BK 21 PLUS Team for Advanced Chemical Materials, and Institute for Plastic Information and Energy Materials, Pusan National University, Busan, 609-735, Republic of Korea. Tel.: +82-51-510-2727; Fax: +82-51-581-2348; E-mail: shjin@pusan.ac.kr*

[‡] *Surface Technology Division, Korea Institute of Materials Science, Changwon 641-831, Republic of Korea; E-mail: smk1017@kims.re.kr*

References

1 L. Nguyen, H. Choi, S.-J. Ko, M. A. Uddin, B. Walker, S. Yum, J.-E. Jeong, M.-H Yun, T. J. Shin, S. Hwang, J. Y. Kim, H. Y. Woo, *Energy Environ. Sci.*, 2014, **7**, 3040.
2 H. G. Kim, B. Kang, H. Ko, J. Lee, J. Shin, K. Cho, *Chem. Mater.* 2015, **27**, 829.
3 S. Yum, T. K. An, X. Wang, W. Lee, M. A. Uddin, Y. J. Kim, T. L. Nguyen, S. Xu, S. Hwang, C. E. Park, H. Y. Woo, *Chem. Mater.*, 2014, **26**, 2147.
4 J. W. Jo, J. W. Jung, H.-W. Wang, P. Kim, T. P. Russell, W.-H. Jo, *Chem. Mater.* 2014, **26**, 4214.
5 X. Guo, J. Quinn, Z. Chen, H. Usta, Y. Zheng, Y. Xia, J. W. Hennek, R. P. Ortiz, T. J. Marks, A. J. Facchetti, *J. Am. Chem. Soc.*, 2013, **135**, 1986.
6 S. Zhang, L. Ye, W. Zhao, D. Liu, H. Yao, J. Hou, *Macromolecules.* 2014, **47**, 4653.
7 J.-M. Jiang, H.-K. Lin, Y.-C. Lin, H.-C. Chen, S.-C. Lan, C.-K. Chang, K.-H Wei, *Macromolecules* 2014, **47**, 70.
8 L. Huo, S. Zhang, X. Guo, F. Xu, Y. Li, J. Hou, *Angew. Chem., Int. Ed.* 2011, **50**, 9697.
9 (a) N. Chakravarthi, K. Kranthiraja, M. Song, K. Gunasekar, P. Jeong, S.-J. Moon, W. S. Shin, I.-N. Kang, J. W. Lee, S.-H. Jin, *Sol. Energy Mater. Sol. Cells*. 2014, **122**, 136. (b) J.-M. Jiang, P. Raghunath, H.-K. Lin, Y.-C. Lin, M. C. Lin, K.-H. Wei, *Macromolecules,* 2014, **47**, 7070.
10 (a) Y. Wang, F. Yang, Y. Liu, R. Peng, S. Chen, Z. Ge, *Macromolecules.* 2013, **46**, 1368. (b) J. Warnan, A. E. Labban, C. Cabanetos, E. T. Hoke, P. K. Shukla, C. Risko, J.-L. Bredas, M. D. McGehee, P. M. Beaujuge, *Chem. Mater.,* 2014, **26**, 2299.
11 M. Zhang, Y. Gu, X. Guo, F. Liu, S. Zhang, L. Huo, T. P. Russell, J. Hou, *Adv. Mater*., 2013, **25**, 4944.
12 J. J. Intemann, K. Yao, H.-L. Yip, Y.-X. Xu, Y.-X. Li, P.-W. Liang, F.-Z. Ding, X. Li, A. K.-Y. Jen, *Chem. Mate*r., 2013, **25**, 3188.
13 J. Subbiah, B. Purushothaman, M. Chen, T. Qin, M. Gao, D. Vak, F. H. Scholes, X. Chen, S. E. Watkins, G. J. Wilson, A. B. Holmes, W. W. H. Wong, D. J. Jones, *Adv. Mater.,* 2014, DOI: 10.1002/adma.201403080.
14 R. Dąbrowski, P. Kula, J. Herman, *Crystals,* 2013, **3**, 443.
15 S. Gauza, C. H. Wen, S. T. Wu, N. Janarthanan, C. S. Hsu, *Jpn. J. Appl. Phys.*, 2004, **43**, 7634.
16 S. Gauza, A. Parish, S.-T. Wu, A. Spadlo, R. Dabrowski, *Mol. Cryst. Liq. Cryst*., 2008, **489**, 135/ [461].
17 J. Hou, L. Huo, C. He, C. Yang, Y. Li, *Macromolecules*, 2006, **39**, 594.
18 P. Schilinsky, U. Asawapirom, U. Scherf, M. Biele, C. J. Brabec, *Chem. Mater*., 2005, **17**, 2175.
19 M. Kopper, C. J. Brabec, S. Heiml, A. Schausberger, W. Duffy, M. Heeney, I. McCulloch, *Macromolecules,* 2009, **42**, 4661.
20 W. Li, L. Yang, J. R. Tumbleston, L. Yan, H. Ade, W. You, *Adv. Mater.,* 2014, **26**, 4456.
21 L. Dou, J. Gao, E. Richard, J. You, C.-C. Chen, K. Cha, Y. He, G. Li, Y. Yang, *J. Am. Chem. Soc*. 2012, **134**, 10071.
22 Y. Li, *Acc. Chem. Res*., 2012, **45**, 723.
23 (a) N. Chakravarthi, K. Gunasekar, C. S. Kim, D.-H. Kim, M. Song, M.; Y. G. Park, J. Y. Lee, Y. Shin, I.-K. Kang, S.-H. Jin, *Macromolecules,* 2015, **48**, 2454. (b) M.-S. Su, C.-Y. Kuo, M.-C. Yuan, U.-S. Jeng, C.-J. Su, K.-H. Wei, *Adv. Mater*., 2011, **23**, 3315.
24 C. Liu, K. Wang, X. Hu, Y. Yang, C.- H. Hsu, W. Zhang, S. Xiao, X. Gong, Y. Cao, *ACS Appl. Mater. Interfaces*., 2013, **5**, 12163.
25 X. Liu, W. Wen, G. C. Bazan, *Adv. Mater*., 2012, **24**, 4505.
26 H. Li, H. W. Tang, L. G. Li, W. T. Xu, X. L. Zhao, X. N. Yang, *J. Mater. Chem*. 2011, **21**, 6563.
27 S. Nam, J. Jang, H. Cha, J. Hwang, T. K. An, S. Park, C. E. Park, *J. Mater. Chem*., 2012, **22**, 5543.
28 Y. Wang, Y. Liu, S. Chen, R. Peng, Z. Ge, *Chem. Mater*., 2013, **25**, 3196.
29 S. Wen, X. Yun, W. Chen, Q. Liu, D. Zhu, C. Gu, M. Sun, R. Yang, *RSC Adv*., 2014, **4**, 58426.
30 P. Sista, H. Nguyen, J. W. Murphy, J. Hao, D. K. Dei, K. Palaniappan, J. Sevello, R. S. Kularatne, B. E. Gnade, B. Xue, P. C. Dastoor, M. C. Biewer, M. C. Stefan, *Macromolecules,* 2010, **43**, 8063.
31 P. Sista, B. Xue, M. Wilson, N. Holmes, R. S. Kularatne, H. Nguyen, P. C. Dastoor, W. Belcher, K. Poole, B. G. Janesko, M. C. Biewer, M. C. Stefan, *Macromolecules,* 2012, **45**, 772.
32 J. Yuan, Z. Zhai, H. Dong, J. Li, Z. Jiang, Y. Li, W. Ma, *Adv. Funct. Mater.,* 2013, **23**, 885.
33 J. Zou, H. L. Yip, S. K. Hau, A. K. Y. Jen, *Appl. Phys. Lett.*, 2010, **96**, 203301.
34 M. Tong, S. Cho, J. T. Rogers, K. Schmidt, B. B. Y. Hsu, D. Moses, R. C. Coffin, E. J. Kramer, G. C. Bazan, A. J. Heeger, *Adv. Funct. Mater*., 2010, **20**, 3959.

35 V. D. Mihailetchi, H. X. Xie, B. de. Boer, L. J. A. Koster, P. W. M. Blom, *Adv. Funct. Mater.*, 2006, **16**, 699.

Graphical Abstract

New 2D π-conjugated polymers based on benzodithiophene unit for efficient and stable organic solar cells